RSC Advances

This is an *Accepted Manuscript*, which has been through the Royal Society of Chemistry peer review process and has been accepted for publication.

Accepted Manuscripts are published online shortly after acceptance, before technical editing, formatting and proof reading. Using this free service, authors can make their results available to the community, in citable form, before we publish the edited article. This *Accepted Manuscript* will be replaced by the edited, formatted and paginated article as soon as this is available.

You can find more information about *Accepted Manuscripts* in the Information for Authors.

Please note that technical editing may introduce minor changes to the text and/or graphics, which may alter content. The journal's standard Terms & Conditions and the Ethical guidelines still apply. In no event shall the Royal Society of Chemistry be held responsible for any errors or omissions in this *Accepted Manuscript* or any consequences arising from the use of any information it contains.

ROYAL SOCIETY
OF CHEMISTRY

www.rsc.org/advances

Kinetic and Thermodynamic Study of Polyaniline Functionalized Magnetic Mesoporous Silica for Magnetic Field Guided Dye Adsorption

Triveni Kumar Mahto, Soumen Chandra, Chanchal Haldar, Sumanta kumar Sahu*

Department of Applied Chemistry, Indian School of Mines, Dhanbad 826004, Jharkhand, India

* To whom correspondence should be addressed. E-mail:sumantchem@gmail.com, sahu.s.ac@ismdhanbad.ac.in; Fax: +91-326-2307772; Tel: +91-326-2235936

ABSTRACT

An eco-friendly magnetic mesoporous silica (MS@Fe_3O_4) with high surface area was fabricated using a colloidal chemical method. Hereafter, polyaniline (Pani) was conjugated into the pores of MS@Fe_3O_4 to obtain Pani-MS@Fe_3O_4 nanocomposites. The nanocomposites were essentially monodispersed and highly efficient for the adsorption of methyl orange (MO). In addition, the rate of the adsorption reaction followed pseudo second order kinetics with the adsorption isotherm well fitted to the Langmuir isotherm model. The negative values of ΔG and positive value of ΔH indicate that the overall adsorption process are spontaneous along with endothermic in nature. The density functional theory (DFT) calculation using Gaussian 09 and GaussView 5.0 program also supported the electrostatic interaction phenomena between Pani and MO which is mainly responsible for adsorption.

KEYWORDS: Polyaniline; Magnetic mesoporous; Electrostatic interaction; Pseudo second order; endothermic.

RSC Advances Accepted Manuscript

1. INTRODUCTION

Over the last two decades mesoporous silica serve as the material of choice in many applications due to their unique characteristics like high surface areas,[1] large pore volumes and uniform pore sizes [2]. Recently, Metal oxide@mesoporous silica core-shell nanocomposites have been extensively used and are widely studied. [3-5] One class of these nanocomposites, mesoporous silica coated Fe_3O_4 nanoparticles, have been recognized as a significant material in many fields including catalysis,[6] biomedical engineering [7] and environmental remediation [8]. Discrete nanocomposite with magnetic core and porous shell structures are of specific attention due to their high surface areas, large amount of accessible pore volume and easy separation by external magnetic field. However, the applications of pure silica materials are limited due to the presence of less number of functional groups on mesopore surface. The surface properties of pure mesoporous silica materials are therefore required to be amended by incorporating species with desired functionalities. The functions of the organic group determine the properties of the mesoporous silica materials such as surface reactivity, adsorption capacity and enhanced stability. A variety of functional groups, such as amino [9], carboxylic acid [10], thiol [11] and sulfonic acid [12] have been introduced into silica matrices for diverse applications. In this investigation, the magnetic mesoporous silica have been functionalized by amine and imine groups through polyaniline modification.

Among the conducting polymers, Polyaniline (Pani) is the most intensively studied candidate for industrial applications due to its easy synthesis, good environmental stability [14], low cost [13] and high conductivity [15]. To date, a number of polyaniline conjugates have been successfully used for diverse applications.[16, 17] For instance, Z. F. Lee et al prepared graphene/polyaniline nanocomposites, where polyaniline were sandwiched between layers of graphene sheets and the nanocomposites were investigated as supercapacitors. [16] U. Bogdanovic et al employed in-situ polymerization technique to synthesized cheaper copper-polyaniline nanocomposite materials and then investigate its antimicrobial properties. [17] But there are few reports on the

RSC Advances Accepted Manuscript

polyaniline modified magnetic mesoporous silica nanocomposites. Therefore, it is necessary to investigate the nanocomposite and their importance. Here we have functionalized Pani on the surface of magnetic mesoporous silica by simple oxidative polymerization technique and subsequently the nanocomposite is applied for adsorption study.

Industrial effluents discharging into hydrosphere are harmful when brought in contact with living tissues for a long time. Dyes, the most harmful industrial effluents, reduce the sunlight penetration into the water bodies and consequently precluding the photosynthesis of aqueous flora and fauna. [18] Dyes are also endangering public health through direct use of polluted water as well as eating aquatic organisms that live in polluted water resources. Different physico-chemical methods have been proposed for the removal of dyes from aqueous solutions. In contrast, the possible techniques, adsorption process, is established as the most attractive and efficient method for the removal of organic dyes from waste water because of its low cost [19], easy operational conditions and better performance. [20] Various adsorbents, such as activated carbon, alumina, metal hydroxide, zeolite, and mesoporous silica have been used to remove azo-dyes from wastewater. [21-23] There is still space to search for a low-cost adsorbent to develop a green, simple and rapid synthesis for organic dye adsorption. In this context, we have developed porous magnetic nanoparticles with high surface area conjugated with Pani for the adsorption of anionic dye. In this study, MO is used as a model effluent compound because it is widely used in textile, papermaking and leather industries and is harmful to the society. [24]

2. MATERIAL AND METHODS

2.1 Materials

$FeCl_3$ (anhydrous), $FeSO_4\cdot 7H_2O$, NH_4OH, tetraethyl orthosilicate (TEOS) and ammonium persulphate (APS), MO, aniline, HCl, ethanol, methanol, benzene, N,N-Dimethyl formamide (DMF), n-hexane and N-Cetyl-N,N,N-trimethyl ammonium bromide (CTAB) were procured

RSC Advances Accepted Manuscript

from Merck. Millipore grade water was employed throughout the experiments. The stock solution of MO was prepared in water and diluted to different required concentrations.

2.2 Methods

The synthesis of Pani-MS@Fe_3O_4 was performed according to our previously reported procedure [25] which was composed of three steps. Firstly, Fe_3O_4 magnetic nanoparticles were synthesized by co-precipitation method. Secondly, core shell (MS@Fe_3O_4) structure was constructed by silica coating and generation of pores on the surface of silica coated magnetic nanoparticles. Finally, polymerization of aniline was performed onto MS@Fe_3O_4 to achieve Pani-MS@Fe_3O_4 nanocomposite.

2.2.1 Synthesis of MS@Fe_3O_4

Fe_3O_4 nanoparticles and MS@Fe_3O_4 nanocomposites were synthesized according to our previously published procedure. [25] For sheer silica coating on Fe_3O_4, the resulting Fe_3O_4 nanoparticles were homogeneously dispersed in a mixture of 80 ml ethanol, 20 ml water and 1 ml concentrated ammonia solution (28%) for 30 minutes. Subsequently, 0.03 g TEOS was dropped to the stirring mixture. After 6 h the product was separated and repeatedly washed with water ethanol mixture. For further generation of pores on the surface of silica coated Fe_3O_4 nanoparticles, the product was redispersed in a solution mixture of 80 ml water, 70 ml absolute ethanol, 0.3 g CTAB and 1.2 ml ammonia solution (28%). After 30 minutes 0.4 g TEOS was added drop wise and stirring was continued further for another 6 h at room temperature. The product was collected using magnetic concentrator and washed repeatedly with water ethanol mixture. Thereafter, CTAB was removed by stirring the obtained product in 105 ml ethanol solution mixture containing 5 ml 2M HCl for 12 h. The MS@Fe_3O_4 core shell nanoparticles were collected using magnetic concentrator and repeatedly washed with ethanol followed by drying at 60 °c.

RSC Advances Accepted Manuscript

2.2.2 Synthesis of Pani-MS@Fe_3O_4

0.1 g MS@Fe_3O_4 nanoparticles were deposited in a mixture of 0.1g aniline and 1 ml hexanol. After 24 h, 0.2 g APS dissolved in 2 ml 1N HCl were added drop wise into the solution under stirring at low temperature, 0-5°c. After 2 h stirring the suspension was displaced to low temperature for 12 h. Finally the product was collected using a magnetic concentrator and washed with ethanol followed by drying at 60 °c.

2.3 Characterization

The surface functional groups of silica coated Fe_3O_4, MS@Fe_3O_4, Pani-MS@Fe_3O_4 and MO adsorbed Pani-MS@Fe_3O_4 were investigated using FTIR spectroscopy (Thermo Nicolet Nexux FTIR (model 870). A Raman spectrum was recorded with a Nicolet Almega XR dispersive raman spectrometer using Nd:YAG laser source of wavelength 532 nm. The phase formation and crystallographic state of these particles were determined using Phillips PW 1710 X-ray diffractometer (XRD) with Ni-filtered Co–Kα radiation (λ= 1.79A°). The morphological characterization was performed using scanning electron microscopy (Jeol Model JSM-6340F) and transmission electron microscopy (Phillips CM 200). The Nitrogen adsorption and desorption isotherms were obtained at 77 K using quantumchrome NOVA 3200e instrument. Prior to adsorption, the samples were degassed properly. EDS analysis was carried out by using oxford instruments (X- Max). The absorption spectra of MO was measured by UV-1800 spectrophotometer with operating voltage of 220-240V/50-60Hz (Shimadzu Corporation).

2.4 Dye Adsorption Study

The experiments in the frame of adsorption were compiled in water phase to investigate the effect of different parameters like, time (1-6 min), initial pH (2-9), temperature (303-323K), initial dye concentration (4-32 mg L^{-1}) and adsorbent dose (0.001-0.005g). In general, 0.003g Pani-MS@Fe_3O_4 nanocomposites was added to 10 ml of MO solution (20 mg L^{-1}) and a shaker (Tarsons Spinix Orbital Shaker) with constant shaking of 180 rpm was used according to

RSC Advances Accepted Manuscript

parameters. But the effect of temperature on adsorption behavior of Pani-MS@Fe_3O_4 was investigated using Rivotek Incubator Shaker with 110 rpm. After equilibrium time, the clear supernatant was collected using magnetic lixiviation and the decrease in absorbance of the supernatant was measured by UV spectrophotometer at 463 nm. The percent dye removal efficiency (R_e) was calculated using the following equation. [26, 27]

$$(R_e)\% = \frac{C_0 - C_e}{C_0} \times 100 \qquad (1)$$

The adsorption capacity of Pani-MS@Fe_3O_4 at equilibrium, q_e (mg g^{-1}), was calculated using the equation.[28]

$$q_e = \frac{C_0 - C_e}{W} \times V \qquad (2)$$

Where C_0 and C_e are the initial and equilibrium liquid phase concentrations (mg L^{-1}) respectively; V is the volume of dye solution taken (L);W is the weight of adsorbent taken (g).

2.5 Dye Desorption Study

The experiments in the frame of desorption were conducted by dispersing the dye adsorbed Pani-MS@Fe_3O_4 in methanol solution containing 4% acetic acid. [26] The percent dye desorption (D_e) were calculated using the equation.

$$(D_e)\% = \frac{\text{Dye desorbed (mg/L)}}{\text{Dye adsorbed (mg/L)}} \times 100 \qquad (3)$$

2.6 Density Functional Theory and AdsorptionEnergy Calculation

Gaussian 09 [29]and GaussView 5.0 [30] program package were used to perform electronic structure calculation and visualization. Ground state electronic structure of Pani and MO was optimized by DFT in its unrestricted forms, employing the STO-3g* level set. Electron correlations were included in DFT calculation using Becke3–Lee–Yang–Parr (B3LYP) procedure [31-33] which includes Becke's gradient exchange corrections, Lee, Yang and Parr correlation functional. [34] No symmetry constrain was imposed during the geometry

RSC Advances Accepted Manuscript

optimization. Absence of imaginary frequencies confirmed that optimized geometries are stable.

Pani, MO and Pani*MO complex were optimized at UBLYP/STO-3g* level of theory. Pani was optimized by putting positive charge on the alternating nitrogen atoms. MO was also optimized by specifying the negative charge on one oxygen atom in SO_3^- group.

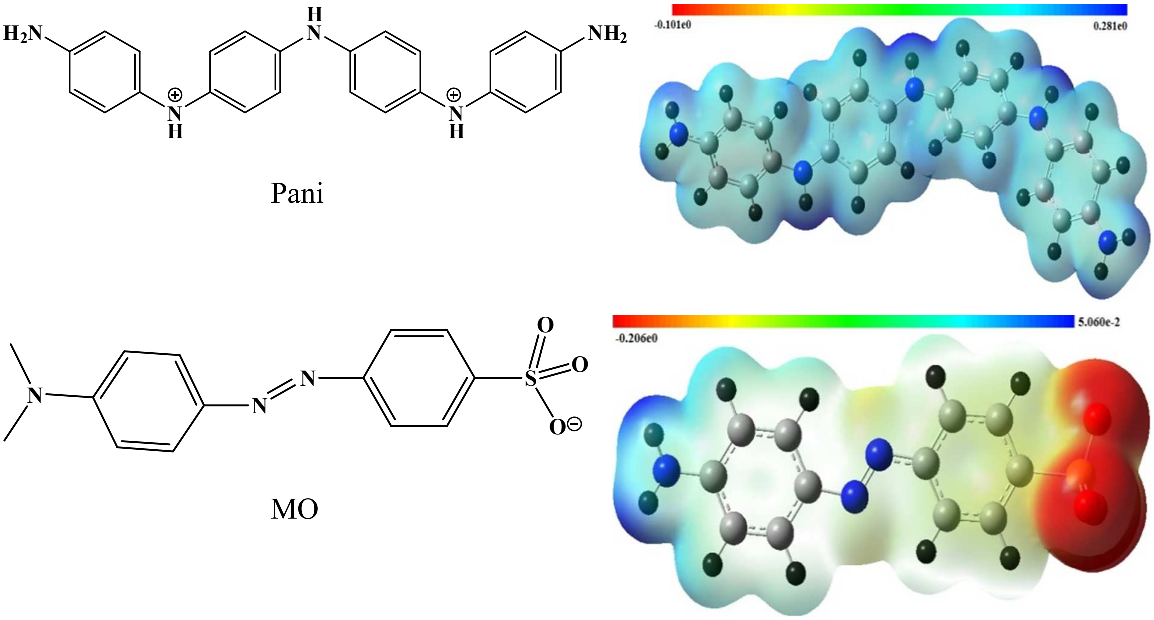

Figure 1: Chemical structure of Pani and MO with corresponding MEP of Pani and MO with iso value 0.004.

To understand the electrophilic and nucleophilic attack of Pani by MO, molecular electrostatic potential map (MEP) of Pani and MO was calculated by using UBLYP/STO-3g* level of theory as shown in the Figure 1. Red color represents the negative diffusion region while blue color represents positive diffusion region. All nitrogen in Pani possess positive diffusion region while in MO negative charge is concentrated on the SO_3^- group. It is clear from Figure 1 that strong attraction acts between N-H groups of Pani and the SO_3^- head of the MO molecule. Optimized structure of the Pani*MO complex, calculated at the same level of theory shown in the Figure 2(a). From the MEP of Pani*MO complex (shown in Figure 2(b)) it is clear that there is an extensive electronic overlap between Pani and MO primarily via 80O-24H-23N.

RSC Advances Accepted Manuscript

Weak interactions are also visible through other oxygen atoms of SO_3^- group and C-H proton of aromatic ring. A high negative complexation energy (-11.05 kcal/mole) confirms the presence of strong interaction between Pani and MO. During the process of optimization proton detached from one of the nitrogen atom (23N) of Pani which subsequently attached to the (80O) SO_3^- group of the MO. A clear picture of 24H shift from 23N to 80O can be visualized by plotting the 23N-24H and 80O-24H bond distance against the optimization steps. Variation of 23N-24H and 80O-24H bond distance with the optimization steps are shown in the Figure S1. Initially 23N-24H bond distance was 1.020 Å, which with increasing the optimization steps, increases and optimize at 1.5097 Å. This signifies the movement of 24H away from the 23N atom. While initially 80O-24H distance was 2.6767Å but with the increasing optimization steps, distance start to reduce and optimized at 1.0838 Å signify the shifting of 24H towards the 80O and formation of 80O-24H bond.

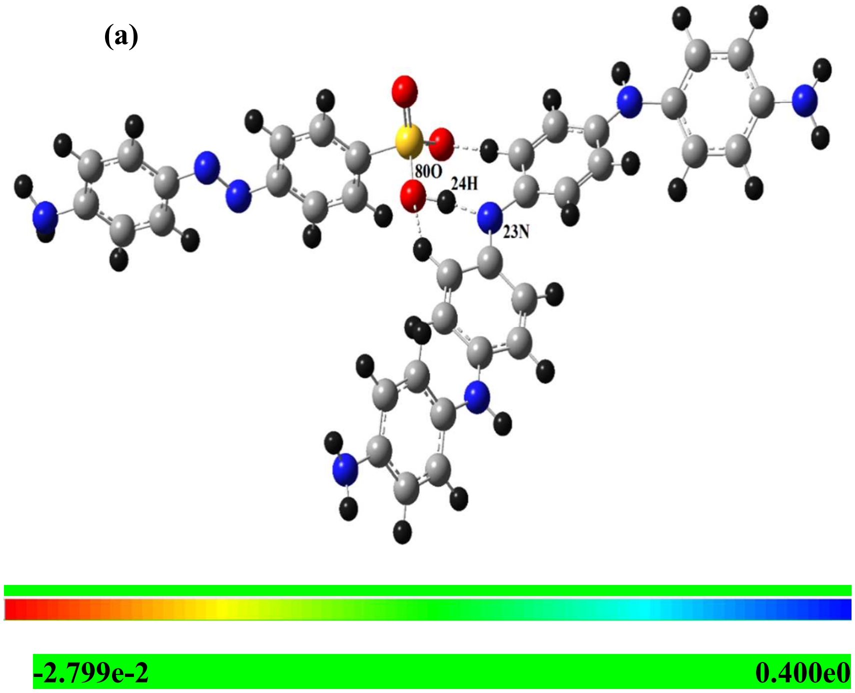

RSC Advances Accepted Manuscript

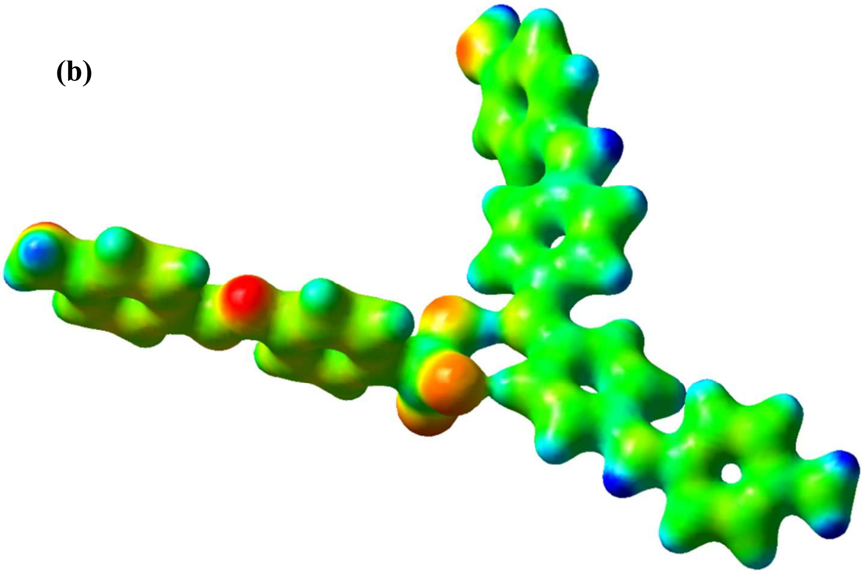

Figure 2: Fully optimized geometry of Pani*MO complex obtained at DFT/UBLYP/STO-3g* level of theory (a), Corresponding MEP at isovalue 0.04 (b).

The interaction energy between the Pani and MO were evaluated by using the following equation

$$\Delta E_{\text{interaction}} \text{ (Pani*MO)} = \text{E (Pani*MO)} - \text{E (Pani)} - \text{E (MO)} \qquad (4)$$

Where $\Delta E_{\text{interaction}}$ (Pani*MO) = formation energy change of Pani*MO complex, E (Pani) = energy of polyaniline and E (MO) = energy of methyl orange and E (Pani*MO) = energy of Pani*MO complex.

Formation of a new O-H bond and presence of a number of electrostatic interactions makes a high change in energy during the complex formation between Pani and MO. The change in energy during the complexation from individual components is 164.4074 kcal/mol. But after the formation of the new complex where MO is protonated and Pani is deprotonated, complexation energy becomes = -25.60 kcal/mole (raw) and = -11.05 kcal/mole (corrected) respectively, with the basis set superposition error (BSSE) corrected interaction energies were 0.023185660755 Hartree.

RSC Advances Accepted Manuscript

3. RESULTS AND DISCUSSION

3.1 Characterization of the magnetic adsorbent

The transmission FTIR spectra of silica coated Fe_3O_4, $MS@Fe_3O_4$, Pani-$MS@Fe_3O_4$, MO adsorbed Pani-$MS@Fe_3O_4$ and MO for the range 4000–400 cm^{-1} has been illustrated in Figure3. In finger print region the characteristic band of Fe-O vibration at 585 cm^{-1} [35] can be associated with the sustainability of magnetic core even after pore formation on silica and MO adsorption. This indicates that magnetic nanoparticles are not affected during washing of CTAB using ethanol HCl mixture. In addition the spectral peak at around 3400 cm^{-1} corresponds to surface-sorbed water or hydroxyl groups.[36, 37] In the spectra of silica related materials, asymmetric and symmetric vibrations of Si–O stretching are observed at 1088 cm^{-1} and 810 cm^{-1} respectively. [38, 39] The characteristic peaks of Pani at 810, 1305, 1494, and 3250 cm^{-1} are attributable to C–H, $C–N^{\bullet +}$, C= C, and N–H bonds respectively for quinoid and benzenoid rings present in Pani. [25, 40] The characteristic peaks at 1235, 1305, and 1581 cm^{-1} indicate that Pani is conjugated in its emeraldine form. [41] The bare MO shows absorption band at 628 cm^{-1} and 810 cm^{-1} are the characteristics of S=O stretching vibration, and C–H aromatic out-of-plane bending respectively. [42] In addition, the N=N stretching band [42] for MO emerges at 1625 cm^{-1}. The emergence of all these bands of MO in Figure 3(e) qualitatively confirms the adsorption of MO into Pani-$MS@Fe_3O_4$ nanocomposites.

RSC Advances Accepted Manuscript

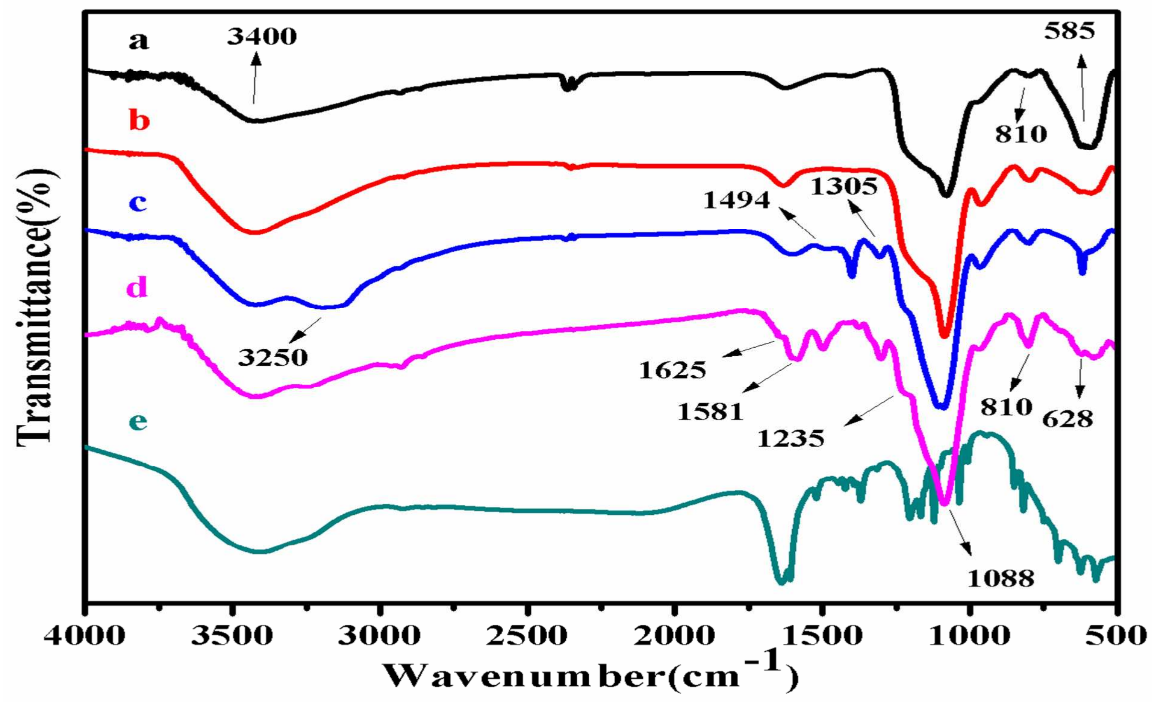

Figure 3: Transmission FTIR spectra of silica coated Fe_3O_4 (a), MS@Fe_3O_4 (b), Pani-MS@Fe_3O_4 (c), MO adsorbed Pani-MS@Fe_3O_4 (d) and MO only (e).

The Raman pattern of Pani-MS@Fe_3O_4 is displayed in Figure 4(a). The spectrum shows three peaks at 410, 440, 512, and 574 cm^{-1} which are attributed to magnetic core. [43, 44] The broad band at 806 cm^{-1} refers to benzene ring deformation. In addition, the strong band appeared at 1587 cm^{-1} is related to C=C stretching vibration in quinonoid ring. The peak of highest intensity at 1488 cm^{-1} is ascribed to C=N stretching vibration of quinonoid ring. The bands at 1334 cm^{-1} and 1166 cm^{-1} corrospond to $C–N^{+\bullet}$vibration of delocalized polaronic structures and C-H bending vibration of semi quinonoid ring.

Figure 4(b-d) show the wide angle XRD patterns of Fe_3O_4, Pani-MS@Fe_3O_4 and MS@Fe_3O_4 respectively, in which the diffraction peaks corresponding to (220), (311), (400), (422), (511), and (440) at 30.1°, 35.8°, 43.1°, 53.6°, 57.09°, and 62.9° can be perfectly indexed to the phase of Fe_3O_4 (Join Committee on Power Diffraction Pattern 75-1609). The matching of diffraction peaks of MS@Fe_3O_4 and Pani-MS@Fe_3O_4 with Fe_3O_4 suggesting that the Fe_3O_4 nanoparticles

RSC Advances Accepted Manuscript

are well retained into the silica matrix. The broad band at 20–25° in Figure 4(c) and 4(d) can be assigned to the amorphous silica shell. Two less intense peaks at 20.2° and 25.08° in Figure 4(c) are due to the slight crystalline nature of as synthesized emeralidine salt form of Pani. [45, 46] Thus FTIR and XRD data corroborate that the as synthesized Pani in Pani-MS@Fe_3O_4 is in the emeralidine salt form.

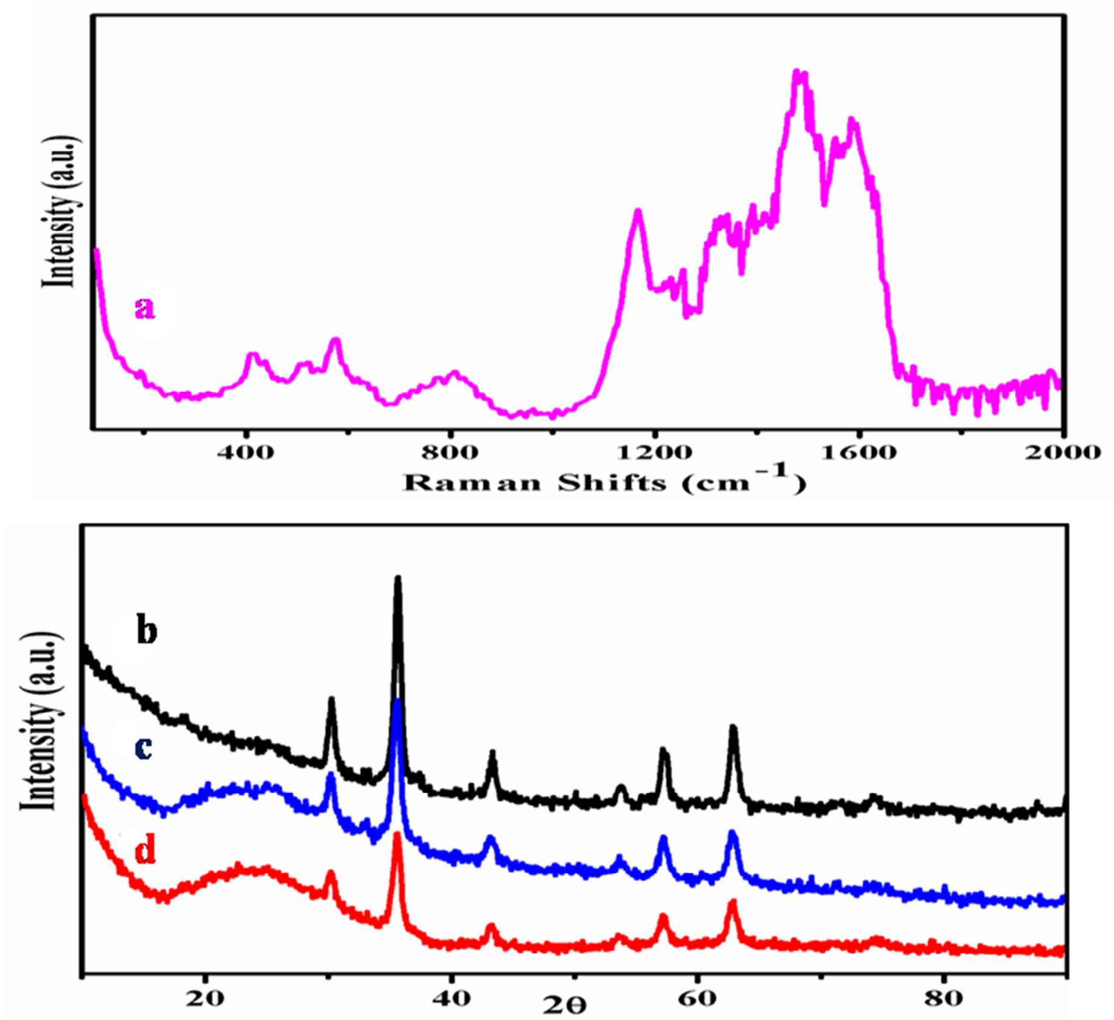

Figure 4: Raman spectra of Pani-MS@Fe_3O_4 (a) XRD patterns of Fe_3O_4 (b) Pani-MS@Fe_3O_4 (c) and MS@Fe_3O_4 (d).

The SEM image of Pani-MS@Fe_3O_4 nanocomposite is shown in Figure 5(a). The as synthesized nanocomposites are regularly spherical with a mean diameter of 160-170 nm and

RSC Advances Accepted Manuscript

rough surface. Additionally, in the TEM image of MS@Fe_3O_4 the inorganic- organic core shell structure can be clearly visualized due to different electron penetrability between the magnetic nanoparticle and silica shell. The black portion refers to the magnetic core while the grey portion with an average thickness of 20-25 nm refers to the silica layer.

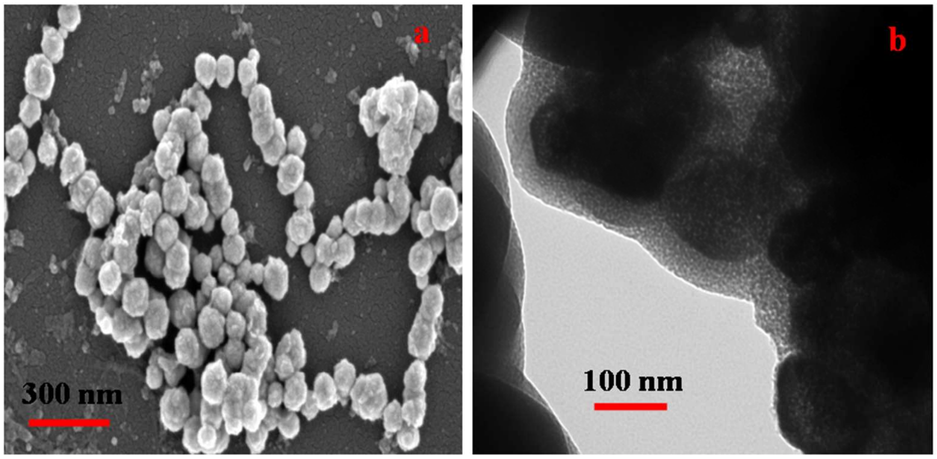

Figure 5: SEM image of Pani-MS@Fe_3O_4 (a) TEM image of MS@Fe_3O_4 (b).

Figure 6 shows the N_2 adsorption/desorption isotherms of MS@Fe_3O_4, Pani-MS@Fe_3O_4, and MO adsorbed Pani-MS@Fe_3O_4. According to the IUPAC classification the isotherms obtained are of typical IV-type isotherms.[47, 48] As expected, the BET surface areas are calculated to be 779.27 m^2/g for MS@Fe_3O_4, 425.65 m^2/g for Pani-MS@Fe_3O_4 [25] and 195.072 m^2/g for MO adsorbed Pani-MS@Fe_3O_4. A possible explanation for the decrease of surface area values is related to the conjugation of Pani into the pores of MS@Fe_3O_4 and further adsorption of MO into Pani-MS@Fe_3O_4.

RSC Advances Accepted Manuscript

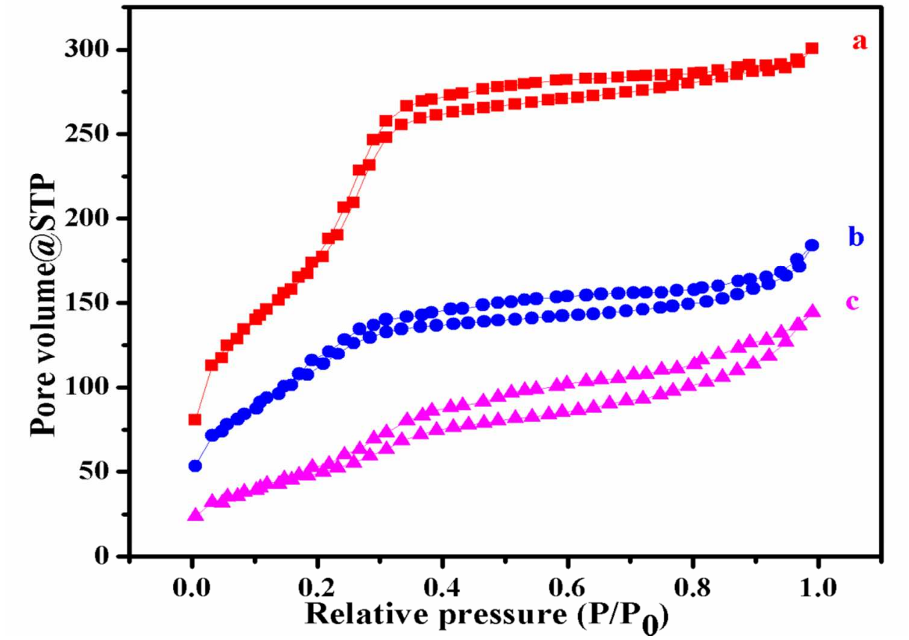

Figure 6: N_2 adsorption-desorption isotherms MS@Fe_3O_4 (a), Pani-MS@Fe_3O_4 (b) and dye adsorbed Pani-MS@Fe_3O_4 nanocomposites (c).

Purity of the Fe_3O_4 core, presence of silica shell, conjugation of Pani and adsorption of MO has been confirmed using EDS technique and the corresponding results for Fe_3O_4, MS@Fe_3O_4, Pani-MS@Fe_3O_4 and MO adsorbed Pani-MS@Fe_3O_4 are shown in Figure 7. The peaks of Fe and O appeared in all spectra corresponds to Fe_3O_4, while the peaks of Si in Figure 7(b-d) could be attributed to the silica coating. The N peak observed in Figure 7(c) is a signature of successful conjugation of Pani into MS@Fe_3O_4. Compared to Pani-MS@Fe_3O_4, MO adsorbed Pani-MS@Fe_3O_4 showed additional peaks of S and Na which confirm the adsorption of MO. The C signals in Figure 7(a-c) could be anticipated for the carbon tap used during sample preparation.

RSC Advances Accepted Manuscript

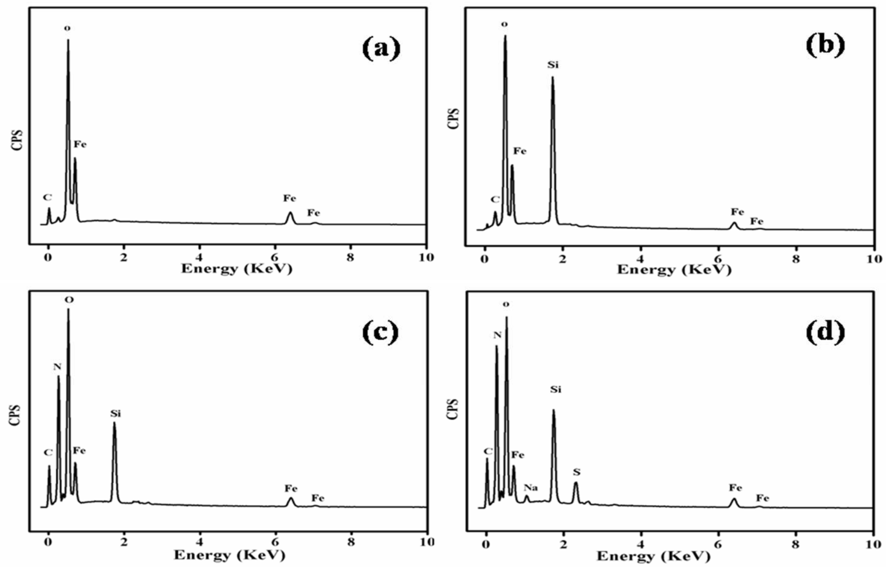

Figure 7: EDS spectra of Fe_3O_4 (a), MS@Fe_3O_4 (b), Pani-MS@Fe_3O_4 (c) and dye adsorbed Pani-MS@Fe_3O_4 (d).

3.2 Effect of pH on Adsorption of MO

Many researchers reported the significant role of pH in adsorption efficacy [49, 50] because it exerts profound influence on the adsorption tendency of the adsorbate molecule presumably due to its influence on the surface charge and functional groups of the adsorbent as well as ionization/dissociation of the adsorbate molecules. [51] In that order, the batch experiments were conducted at different pH ranges from 2.0 to 9.0 at room temperature and the effect of pH on the percentage removal of MO, is shown in Figure 8(a and b).Variable pH was obtained by adding requisite amount of 0.1M HCl or 0.1M NaOH. Results indicate that the adsorption of MO into Pani-MS@Fe_3O_4 is fairly pH dependent and the maximum adsorption efficiency (96.96%) was achieved at pH 4. The p*K*a value of MO is reported 3.4 and at pH <p*K*a, MO predominantly exist in anionic form and subsequently it gets protonated. On the other hand due to the basic nature of nitrogen containing functionalities (imine group --N=, p*K*a= 2.5 and amine group --N=, p*K*a= 5.5), [52] Pani gets positively charged in acidic medium. It is therefore,

RSC Advances Accepted Manuscript

at pH 2 and pH 3, electrostatic repulsion occurred between the positively charged nanocomposites and protonated MO, results in a decline in adsorption (63.1% at pH 342.5% at pH 2 and). However MO, at pH>p*k*a, exists in anionic form and maximum adsorption (96.96%) was achieved at 4. This is due to intensive electrostatic attraction established between positive part of Pani and anionic MO. Above pH 4 adsorption declines gradually up to pH 7 and then minor decreased to become almost constant above pH 8. The competitive adsorption of hydroxyl on imine and amine groups might result in electrostatic repulsion with anionic MO, leading to low adsorption of MO at basic pH.

3.3 Effect of MO Dose on Adsorption

Figure 8(c) shows the effect of the increment of concentration of dye on the % adsorption of Pani-MS@Fe_3O_4 nanocomposites. Results indicate that dye adsorption declined from 99.12% to 90.35% with an increase in dye concentration from 4 mg/l to 32 mg/l of dye. It is due to the decrease in the availability of effective adsorption sites on adsorbent. [45]

3.4 Effect of Adsorbent Dose on Adsorption

The effect of adsorbent dosage on the adsorption of MO was evaluated using quantities of Pani-MS@Fe_3O_4 adsorbent ranging from 0.001g to 0.005g. Experimental data, as shown in Figure 8(e), reveal that the MO adsorption was found to be lowest (77.45%) at 0.001g adsorbent dose and sharply increases to 97.42% at adsorbent dose 0.003g. Above this adsorbent dose, the adsorption becomes almost constant. Initially the increase in percentage adsorption with increment of adsorbent is attributed to higher available surface area, consequently augmenting the number of active sites [54], available for MO adsorption [55]. On contrary, the almost constant percentage of MO adsorption obtained from adsorbent dose, 0.003g, is due to the aggregation of active sites of adsorbent. Therefore we fixed the adsorbent dose at 0.003g.

RSC Advances Accepted Manuscript

3.5 Effect of Temperature on Adsorption of Dye

Temperature is another important parameter that affects the adsorption process by changing the diffusion rate of the adsorbate molecules, owing to decrease in the viscosity of the solution. Moreover, it alters the equilibrium adsorption capacity (q_e) of the adsorbent. [56] So this section of experiments is carried out at five different temperatures viz., 303K, 308K, 313K, 318K and 323K. The observed values are shown in Figure 8(c). As the temperature increases removal efficiency of dye increases and consequently q_e increases. The thermodynamic parameters are also calculated using adsorption study under different temperature conditions.

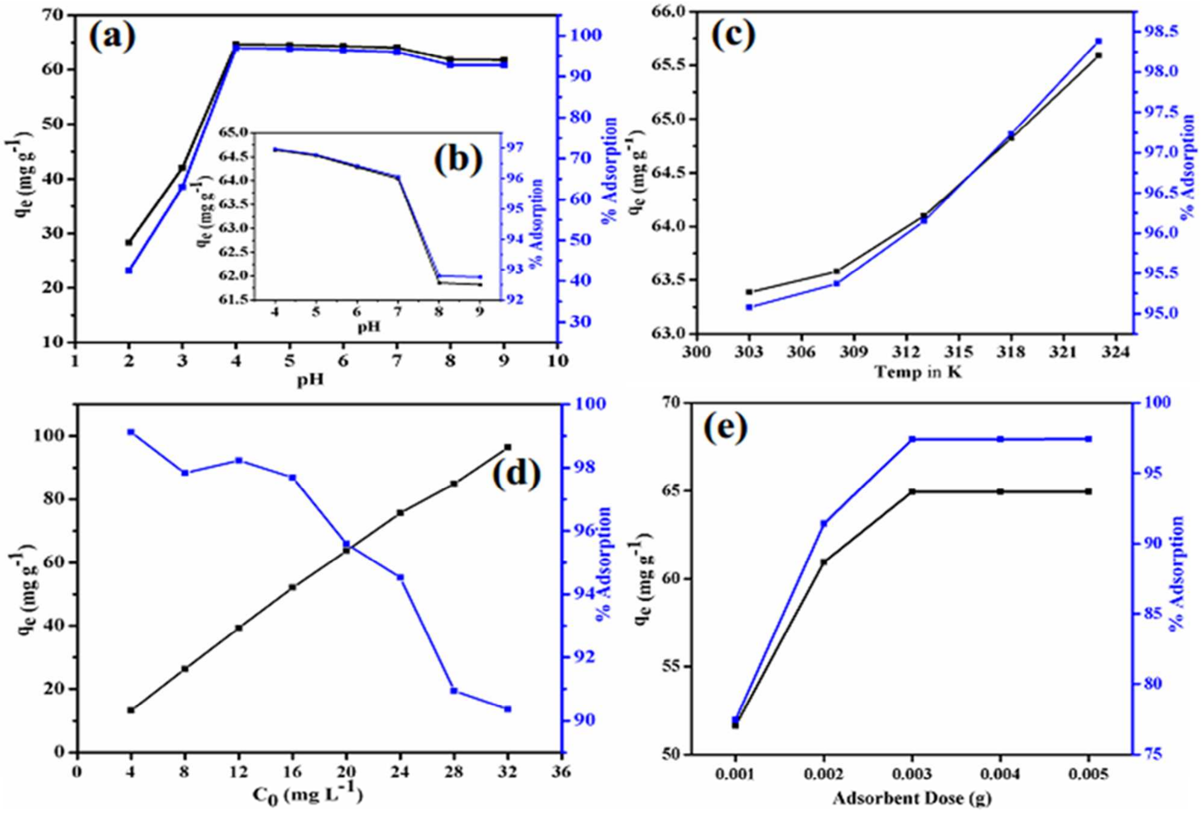

Figure 8: Effect of pH (a); Inset is the effect of pH in the range pH 4 to pH 9 (b);Temperature (c); initial MO concentration on the adsorption of MO on Pani-MS@Fe_3O_4 and (d) Mass of adsorbent (e). {Temperature: 273K- For (a), (b), (d) and (e), Initial MO concentration: 20 mg L^{-1}(10 ml)- For (a), (b), (c) and (e). Pani-MS@Fe_3O_4: 0.003g- For (a), (b), (c) and (e).}.

RSC Advances Accepted Manuscript

3.6 Determination of Kinetic Parameters

The dye adsorption process also depends on the contact time between the adsorbate and adsorbent in dispersion as well as on diffusion processes. During adsorption the dye molecules migrate to the outer surface of the adsorbent, diffuse in the boundary layer and consequently settled down into the available internal sites. [57] However the electrostatic interaction between the positive charges of Pani-MS@Fe_3O_4 nanocomposites and negative charges of MO dye is responsible for the adsorption of dye. So the adsorption with respect to time is investigated in terms of, pseudo first order, and pseudo second order models. The condensed graph of these kinetic models is presented in Figure 9. Moreover; the kinetic parameters with their values for the above models are summarized in Table1.The highest value of R^2 (0.999) and lowest value of $\chi2$ (0.00394) for pseudo second order kinetics among the kinetic models reveals that the adsorption of MO into Pani-MS@Fe_3O_4 follows pseudo second order kinetics. In addition, the calculated q_e (66.62 mg g^{-1}) for pseudo second order is very close to q_e (65.13 mg g^{-1}) calculated experimentally. The linear form of pseudo second order model is expressed by the equation,

$$\frac{t}{q_t} = \frac{1}{K_2 q_{e^2}} + \frac{t}{q_e} \qquad (4)$$

Where K_2 (g mg^{-1} min^{-1}) is the adsorption rate constant for pseudo second order, q_t is adsorption capacity at time t and q_e is adsorption capacity at equilibrium. The values of parameters like K_2, q_e, R^2 (correlation coefficient) and $\chi2$ are calculated from the graph t/q_t vs t and tabulated in Table 1. In addition, the Lagergren pseudo first-order kinetic model is expressed as.

$$\ln(q_e - q_t) = \ln q_e - K_1 t \qquad (5)$$

RSC Advances Accepted Manuscript

Where K_1 (min^{-1}) is the adsorption rate constant for Pseudo first order. The values of parameters like K_1, q_e, R^2 and $\chi 2$ are calculated from the graph plotted by taking time against ln (q_e-q_t) and tabulated in the same Table1.

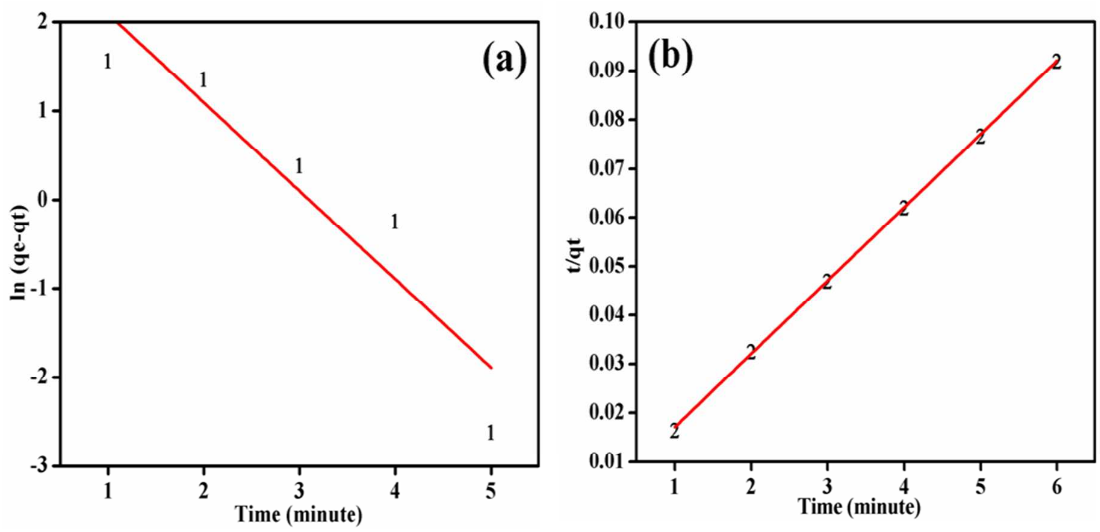

Figure 9: Regression of kinetic plots for MO: Pseudo first order model (a), Pseudo second order (b) {Temperature: 273K, Initial MO concentration: 20 mg L^{-1}(10 ml) and Pani-MS@Fe_3O_4: 0.003g}.

Table 1: Kinetic Parameters for MO Adsorption.

		Pseudo first order			Pseudo second order		
	q_e,exp (mg g^{-1})	q_e,cal (mg g^{-1})	k_1 (min^{-1})	R^2	q_e,cal (mg g^{-1})	k_2 g mg^{-1} min^{-1}	R^2
MO	65.13	21.9	0.99	0.83	66.62	0.002	0.999

3.7 Determination of Isothermic Parameters

The adsorption isotherms are important tool to optimize the distribution of dye molecules between the solid phase and liquid phase. [58] Various classic and non-classic isotherm models like Langmuir, Freundlich, Tempkin and Dubinin-Radushkevish are used to investigate the

RSC Advances Accepted Manuscript

nature of electrostatic adsorption of dye molecules into the adsorbents. [59] The linear fittings for these isotherm models are shown in Figure 10. From the values of R^2 it can be concluded that the adsorption data are found to agree best with the Langmuir model. This observation is akin to different previous reports. [51, 58, 60, 61] The Langmuir model can be presented by

$$\frac{1}{q_e} = \frac{1}{q_0} + \frac{1}{K_l\, q_0\, C_e} \qquad (6)$$

Where q_0 (mg g^{-1}) and K_l are maximum adsorption capacity and the Langmuir constant related to heat of adsorption respectively. [59, 62] The essential characteristics of Langmuir model can be expressed in terms of the separation factor (R_L) which can be presented as

$$R_L = \frac{1}{1 + K_l C_0} \qquad (7)$$

The value of R_L value is the indicative of the adsorption process: for favorable ($0 < R_L < 1$) unfavorable ($R_L > 1$), and linear ($R_L = 1$). Table 2 indicates that the adsorption of MO into Pani-MS@Fe_3O_4 is favorable.

The Frendluich isotherm model is based on the assumption of multilayer adsorption of adsorbate on adsorbent surface. The linearised Freundlich isotherm is expressed by. [57]

$$\ln q_e = \ln K_f + \frac{1}{n} \ln C_e \qquad (8)$$

Where K_f and n are Freundlich constant and heterogeneity factor respectively. The values of 'K_f and n' are calculated from the intercept and slope of the linear plot of ln C_e against ln q_e and are shown in Table 2. The value of 1/n indicate the type of isotherm to favorable (1/ n= 0.41). The linear form of Tempkin isotherm model is expressed by

RSC Advances Accepted Manuscript

$$\mathrm{q_e = B\ln K_t + B\ln C_e} \qquad (9)$$

Where K_t is Tempkin isotherm constant corresponding to maximum binding energy. B = RT/β is also a constant, associated with heat of adsorption β (J mol^{-1}). [63] R and T are the gas constant (8.314 J/mol K) the absolute temperature (K) respectively. A plot of ln C_e versus q_e produces a straight line indicating the uniform distribution of binding energy for MO and adsorbent interaction. Tempkin parameters, B (mg g^{-1}) and K_t (mg L^{-1}) are calculated from the slope and intercept respectively. [53] Dubinin–Radushkevich isotherm model is usually applied for description of adsorption processes on porous adsorbents. [63] The linear form of Dubinin–Radushkevich is expressed by

$$\ln q_e = \ln q_d - D\varepsilon^2 \qquad (10)$$

Where q_d is the theoretical maximum capacity (mg g^{-1}) and D is the parameter related to adsorption energy E, [$\mathrm{E = \frac{1}{\sqrt{2D}}}$]. E demonstrated the information of adsorption nature. If E<8 kJ mol^{-1}, the adsorption is physical in nature, whereas if 8≤E≤16 kJ mol^{-1}, the adsorption in chemical in nature. [64, 65] The calculated value of E, as shown in table 2, suggested that the adsorption is physical in nature. ε^2 is the Polanyi potential which is equal to:

$$\varepsilon = \mathrm{RT\ln[1 + \frac{1}{C_e}]} \qquad (11)$$

The values of D and ln q_d are calculated from the slope and intercept of the linear plot of ln q_e against ε^2 and are shown in Table 2.

RSC Advances Accepted Manuscript

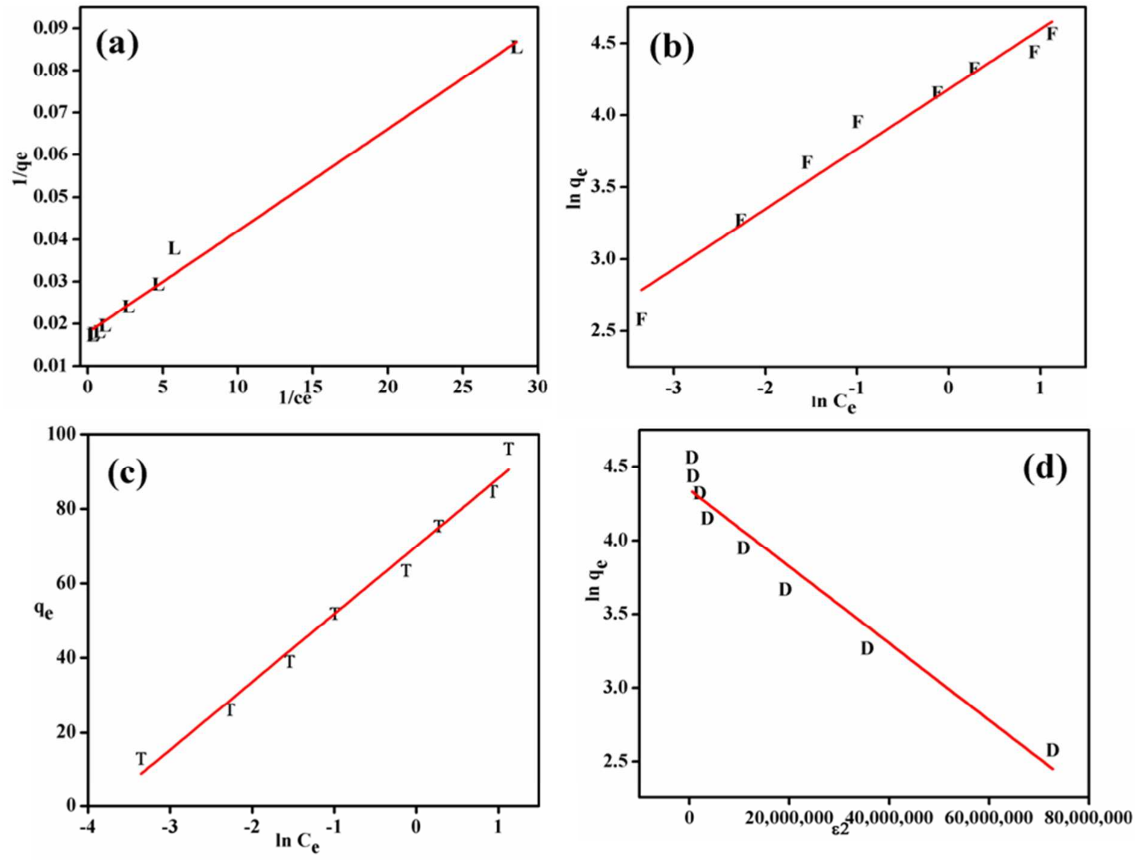

Figure 10: Langmuir (a), Frendluich (b), Tempkin (c) and Dubinin–Radushkevich (d) isotherms for MO adsorption on Pani-MS@Fe_3O_4. {Temperature: 273K, Initial MO concentration: 4-32 mg L^{-1}(10 ml) and Pani-MS@Fe_3O_4: 0.003g}.

Table 2: Adsorption Isotherm for MO Adsorption.

Frendluich		Langmuir
K_f (mg g^{-1}) =65.43	0.956=R^2=0.990	K_l (L mg^{-1}) =0.134
n=2.39		q_0 (mg g^{-1}) =55.74
Tempkin		Dubinin-Radushkevish
K_t (L g^{-1})= 46.66	0.983=R^2=0.780	E(kJ mol^{-1})=0.43
β (J mol^{-1})=5.30		Q_d (mg g^{-1}) =75.50
B= 18.21		D=2.60

RSC Advances Accepted Manuscript

3.8 Determination of Thermodynamic Parameters

The various thermodynamic parameters such as change in Gibbs energy (ΔG: kJ mol^{-1}), entropy (ΔS: kJ $mol^{-1}K^{-1}$) and enthalpy (ΔH: kJ mol^{-1}) are calculated using the formulae given below [57, 58]

$$K_c = \frac{q_e}{C_e} \qquad (12)$$

$$\Delta G = -RT\ln K_c \qquad (13)$$

$$\ln K_c = \frac{\Delta S}{R} - \frac{\Delta H}{RT} \qquad (14)$$

where K_c is distribution coefficient for adsorption, T is temperature in Kelvin, and R (8.314 J mol K^{-1}) is the gas constant. The values of ΔH and ΔS are determined from the slopes and intercepts respectively of the plot of ln K_c against 1/T (Figure 11). The calculated value of ΔG, ΔS and ΔH are shown in Table 3. The obtained negative values of ΔG at each temperature demonstrate the feasibility and spontaneity of the adsorption process. [65, 66] The positive value of ΔH and ΔS substantiate that the adsorption process is endothermic in nature. This observation is akin to many previous research reports.[59, 66, 67] Moreover, the positive value of ΔS reflects the affinity of the adsorbent for MO dyes. [59, 60]

RSC Advances Accepted Manuscript

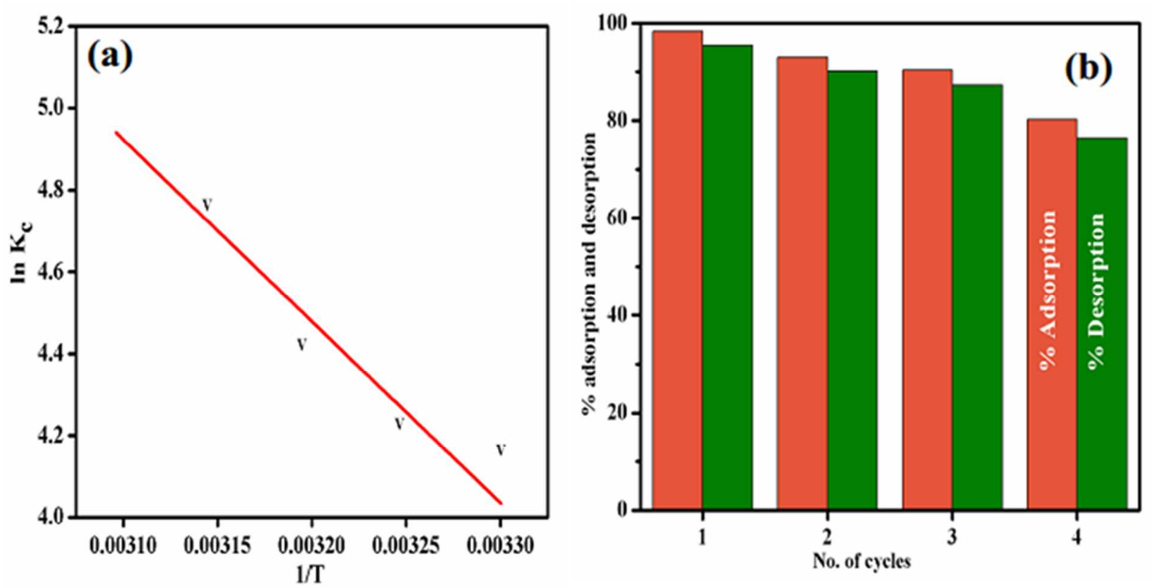

Figure11: Van’t Hoff plot for the adsorption of MO.{Initial MO concentration: 20 mg L^{-1}(10 ml), Pani-MS@Fe_3O_4: 0.003g. For (b)-Initial MO concentration: 40 mg L^{-1}(10 ml) and Pani-MS@Fe_3O_4: 0.01g}.

Table3: Thermodynamic Parameters for MO Adsorption

Temperature (K)	ΔH (kJ mol^{-1})	ΔS (kJ $mol^{-1}K^{-1}$)	K_c	ΔG (kJ mol^{-1})
303	45.79	0.18	63.38	-10.49
308			68.63	-10.82
313			83.24	-11.50
318			117.13	-12.59
323			203.12	-14.26

RSC Advances Accepted Manuscript

3.9 Effect of Reuse of Adsorbent on Adsorption of MO

The regeneration of adsorbent with having stability and adsorption ability is important features for its practical application. So the regeneration of adsorbent is investigated here and the graph is shown in Figure 12(b). The investigation implied that 80.25 percent of dye can be adsorbed even in fourth cycle. Furthermore, after four cycles of the adsorption-desorption process, the Pani-MS@Fe_3O_4 nanocomposite could be easily separated under an external magnetic bar, indicating the high stability of Pani-MS@Fe_3O_4.

4. CONCLUSION

In this work, the organic moieties, Polyaniline, were incorporated into the pores of MS@Fe_3O_4 to obtain the nanocomposite based adsorbent, Pani-MS@Fe_3O_4. The FTIR analysis, surface area measurement and EDS spectra proved the adsorption of MO into the synthesized adsorbent. The removal efficiency of MO is dependent on initial pH and temperature of the medium. The maximum dye adsorption takes place at pH 4. In chemistry point of view the electrostatic interaction between the positive charges of Pani-MS@Fe_3O_4 and negative charges of MO dye is responsible for the adsorption of dye. The adsorbent is technically feasible as it could be easily separated magnetically after four adsorption- desorption cycles.

Acknowledgement

The authors would like to acknowledge their institute, Indian School of Mines, Dhanbad for fundamental research support.

References

[1] T. Li, Z. Shu, J. Zhou, Y. Chen, D. Yu, X. Yuan, and Y. Wang, Appl. Clay. Sci. 2015, **107**, 182-187.

[2] H. Zheng, D. Hu, L. Zhang, C. Ma, and T. Rufford, Miner. Eng. 2012, **35**, 20-26.

RSC Advances Accepted Manuscript

[3] X. Zhang, T. Zeng, S. Wang, H. Niu, X. Wang, and Y. Cai, J. Colloid Interface Sci., 2015, **448**, 189-196.

[4] H. Tong, N. Enomoto, M. Inada, Y. Tanaka, and J. Hojo, Electrochim. Acta, 2014, **130,** 329-334.

[5] D. Yang, K. Wei, Q. Liu, Y. Yang, X. Guo, and H. Rong, Mater. Sci. Eng., C, 2013, **33,** 2879-2884.

[6] Y. Chen, F. Zhang, Y. Fang, X. Zhu, W. Zhen, R. Wang, and J. Ma, Catal. Commun. 2013, **38**, 54-58.

[7] E. Che, L. Wan, Y. Zhang, Q. Zhao, X. Han, J. Li, and J. Liu, Asian J. Pharma. Sci., 2014, **9**, 317-323.

[8] S. Wang, K. Wang, C. Dai, H. Shi, and J. Li, Chem. Ing. J., 2015, **262**, 897-903.

[9] H. Gu, Y. Guo, S. Y. Wong, Z. Zhang, X. Ni, Z. Zhang, W. Hou, C. He, V. P. W. Shim, and X. Li, Microporous Mesoporous Mater., 2013, **170**, 226-234.

[10] J. R. Deka, D. Saikia, Y. S. Lai, C. H. Tsai, and W. C. Chang, Microporous Mesoporous Mater., 2015, In press: http://dx.doi.org/10.1016/j.micromeso.2015.04.015

[11] D. Liu, J.H. Lei, L. P. Guo, X. D. Du, and K. Zeng, Microporous Mesoporous mater., 2009, **117,** 67-74.

[12] E. M. Usai, M. F. Sini, D. Meloni, V. Solinas, and A. Salis, Microporous Mesoporous Mater., 2013, **179**, 54-62.

[13] T. T. Duong, T. Q. Tuan, D. V. A. Dung, N. V. Quy, D. L. Vu, M. H. Nam, N. D. Chien, S. G. Yoon, and A. T. Le, Current Appl. Phy. 2014, **14**, 1607-1611.

[14] K. H. Park, S. J. Kim, R. Gomes, and A. Bhaumik, 2015, **260,** 393-398.

[15] V. Janaki, B. T. Oh, K. Shanthi, K. J. Lee, and A. K. Ramasamy, Synth. Met., 2014, **162**, 974-980.

[16] Z. F. Li, H. Zhang, Q. Liu, L. Sun, L. A. Stanciu, and J. Xie, ACS Appl. Mater. Interfaces, DOI: 10.1021/am4001634.

RSC Advances Accepted Manuscript

[17] U. Bogdanovic, V. Vodnik, M. Mitric, S. Dimitrijevic, S. D. Skapin, V. Zunic, M. Budimir, and M. Stoiljkovic, Appl. Mater. Interfaces, 2015, **7**, 1955-1966.

[18] V. K. Gupta, and Suhas, J. Environ. Manage. 2009, **90**, 2313-2342.

[19] R. Salehi, M.Arami, and N. M. Mahmoodi, Colloids Surf. B., 2010, **80**, 86-93.

[20] L.Yu, and Y. M. Luo, Journal of Environmental Chemical Engineering, 2014, **2**, 220-229.

[21] M. T. Yagub, T. K. Sen, S. Afroze and H. M. Ang, Adv. Colloid Interface Sci., 2014, **209**, 172-184.

[22] B. Yahyaei and S. Azizian, Chem. Enj. J.,2012, **209**, 589-596.

[23] L. Tang, Y. Cai, G. Yang, Y. Liu, G. Zeng, Y. Zhou, S. Li, J. Wang, S. Zhang, Y. Fang and Y. He, Appl. Surf. Sci.,2014, **314**, 746-753.

[24] L. Wang, X. L. Wu, W. H. Xu, X. J. Huang, J. H. Liu and A. W. Xu, ACS Appl. Mater. Interfaces., 2012, **4**, 2686-2692.

[25] T. K. Mahto, A. R. Chowdhuri, B. sahoo and S. K. Sahu, Polym. Compos., DOI: 10.1002/pc.23278.

[26] T. K. Mahto, A. R. Chowdhuri and S. K. Sahu, J. Appl. Polym. Sci., 2014, 131, 40840-40848.

[27] L. Wang, X. L. Wu, W. H. Xu, X. J. Huang, J. H. Liu and A. W. Xu, ACS Appl. Mater. Interfaces., 2012, **4**, 2686-2692.

[28] J. Goscianska, M. Marciniak and R. Pietrzak, Chem. Eng. J., 2014, **247**, 258-264.

[29] M. J. Frisch; et al., GAUSSIAN 09, Rev. D.01, Gaussian, Inc., Wallingford, CT, 2009.

[30] R. D. II, Dennington, T.A. Keith and J.M. Millam, GaussView 5.0, Wallingford, CT, 2009.

[31] A. D. Becke, J. Chem. Phys., 1993, **98**, 5648-5652.

[32] C. Lee, W. Yang and R.G. Parr, Phys. Rev. B, 1988, 37,785.

RSC Advances Accepted Manuscript

[33] B. D. Becke, Phys. Rev. B, 1988, **38**, 3098.

[34] S. H. Vosko, L. Wilk and M. Nusair, Can. J. Phys., 1980, 58, 1200.

[35] S. Liu, S. Li, H. Niu, T. Zeng, Y. Cai, C. Shi, B. Zhou, F. Wu, and X. Zhao, Microporous Mesoporous Mater., 2014, **200**, 151-158.

[36] B. Sahoo, K. S. P. Devi, S. Dutta, T. K. Maiti, P. Pramanik and D. Dhara, J. Colloid Interface Sci., 2014, **431**, 31-41

[37] Y. Hu, S. Tang, L. Jiang, B. Zou, J. Yang, and H. Huang, Process. Biochem. 2012, **47**, 2291-2299.

[38] X. Wang, Y. Liu, S. Wang, D. Shi, X. Zhou, C. Wang, J. Wu, Z. Zeng, Y. Li, J. Sun, J. Wang, L. Zhang, Z. Teng, and G. Lu, App. Surf. Sci. 2015, **332**, 308-317.

[39] E. V. Garcia, E. M. O. Moya, J. A. Cecilia, C. L. Cavalcante Jr., J. J. Jimenez, D. C. S. Azevedo, and E. R. Castellon, Microporous Mesoporous Mater., 2015, **209,** 172-183.

[40] W. Yao, C. Shen, and Y. Lu, Compos. Sci. Technol. 2013, **87**, 8-13.

[41] L. Tang, Y. Fang, Y. Pang, G. Zeng, J. Wang, and Y. Zhou, Chem. Eng. j., 2014, **254**, 302-312.

[42] L. Ayed, E. Khelifi, H. B. Jannet, and H. Miladi, Chem. Eng. J. 2010, **165**, 200-208.

[43] M. Balaji, P. C. Lekha and D. P. Padiyan, Vib. Spectrosc., 2012, **62**, 92-97.

[44] L. Wang, Y. Huang, C. Li, J. Chen and X. Sun, Synth. Met., 2014, **198**, 300-307.

[45] U. Bogdanovic, V. V. Vodnik, S. P. Ahrenkiel, M. Stoiljkovic, G. C. Marjanovic, and J. M. Nedeljkovic, Synth. Met., 2014, **195**, 122-131.

[46] V. Janaki, K. Vijayaraghavan, B. T. Oh, K. J. Lee, K. Muthuchelian, A. K. Ramasamy, and S. K. Kannan, Carbohydr. Polym. 2012, **90**, 1437-1444.

[47] M. Xie, H. Shi, Z. Li, H. Shen, K. Ma, B. Li, S. Shen, and Y. Jin, Colloids Surf., B 2013, **110**, 138-147.

[48] P. B. Sarawade, J. K. Kim, A. Hilonga, H. T. Kim, J. Hazard. Mater., 2010, **173**, 576-580.

RSC Advances Accepted Manuscript

[49] L. Ai, C. Zhang, and Z. Chen, J. Hazard. Mater., 2011, **192**, 1515-1524.

[50] J. S. Piccin, G. L. Dotto, M. L. G. Vieira and L. A. A. Pinto, J. Chem. Eng. Data, 2011, **56**, 3759-3765.

[51] M. Anbia, S. A. Hariri and S. N. Ashrafizadeh, Appl. Surf. Sci., 2010, **256**, 3228-3233.

[52] A. Zieba, A. Drelinkiewicz, E.N. Konyushenko, and J. Stejskal, Appl. Catal., A. 2010, **383**, 169-181.

[53] S. Ghorai, A. Sarkar, M. Raoufi, A. B. Panda, H. Schönherrand S. Pal, ACS Appl. Mater. Interfaces 2014, **6**, 4766-4777.

[54] N. F. Cardoso, R. B. Pinto, E. C. Lima, T. Calvete, C. V. Amavisca, B. Royer, M. L. Cunha, T. H. M. Fernandes, I. S. Pinto, Desalination, 2011, **269**, 92-103.

[55] B. Royer, N. F. Cardoso, E. C. Lima, T. R. Macedo, C. Airoldi, J. Hazard. Mater., 2010, **181**, 366-374.

[56] N. M. Mahmoodi, B. Hayati and M. Arami, J. Chem. Eng. Data, 2010, **55**, 4638-4649.

[57] C. Klett, A. Barry, I. Balti, P. Lelli, F. Schoenstein and N. Jouini, Journal of Environmental Chemical Engineering, 2014, **2**, 914-926.

[58] N. M. Mahmoodi, B. Hayati, M. Arami and C. Lan, Desalination, 2011, **268**, 117-125.

[59] I. Chaari, M. Feki, M. Medhioub, J. Bouzid, E. Fakhfakh, and F. Jamoussi, J. Hazard. Mater., 2009, **172**, 1623-1628.

[60] P. Sharma and M. R. Das, J. Chem. Eng. Data, 2013, **58**, 151-158.

[61] L. Wang, X. L. Wu, W. H. Xu, X. J Huang, J. H. Liu and A. W. Xu, ACS Appl. Mater. Interfaces, 2012, **4**, 2686-2692.

[62] G. Annadurai, L. Y. Ling and J. F. Lee, J. Hazard. Mater., 2008, **152**, 337-346.

[63] V. V. Panic and S. J. Velickovic, Sep. Purif. Technol., 2014, **122**, 384-394.

RSC Advances Accepted Manuscript

[64] U. R. Malik, S. M. Hasany and M. S. Subhani, Talanta, 2005, **66**, 166-173.

[65] X. Peng, D. Huang, T. O. wubah, D. Fu, J. Huang and Q. Qin, J. Colloid Interface Sci., 2014, **430**, 272-282.

[66] L. Tang, Y. Cai, G. Yang, Y. Liu, G. Zeng, Y. Zhou, S. Li, J. Wang, S. Zhang, Y. Fang and Y. He, Appl. Surf. Sci., 2014, **314**, 746-753.

[67] N. M. Mahmoodi, B. Hayatiand M. Arami, J. Chem. Eng. Data, 2010, **55**, 4638-4649.

RSC Advances Accepted Manuscript

Graphical Abstract

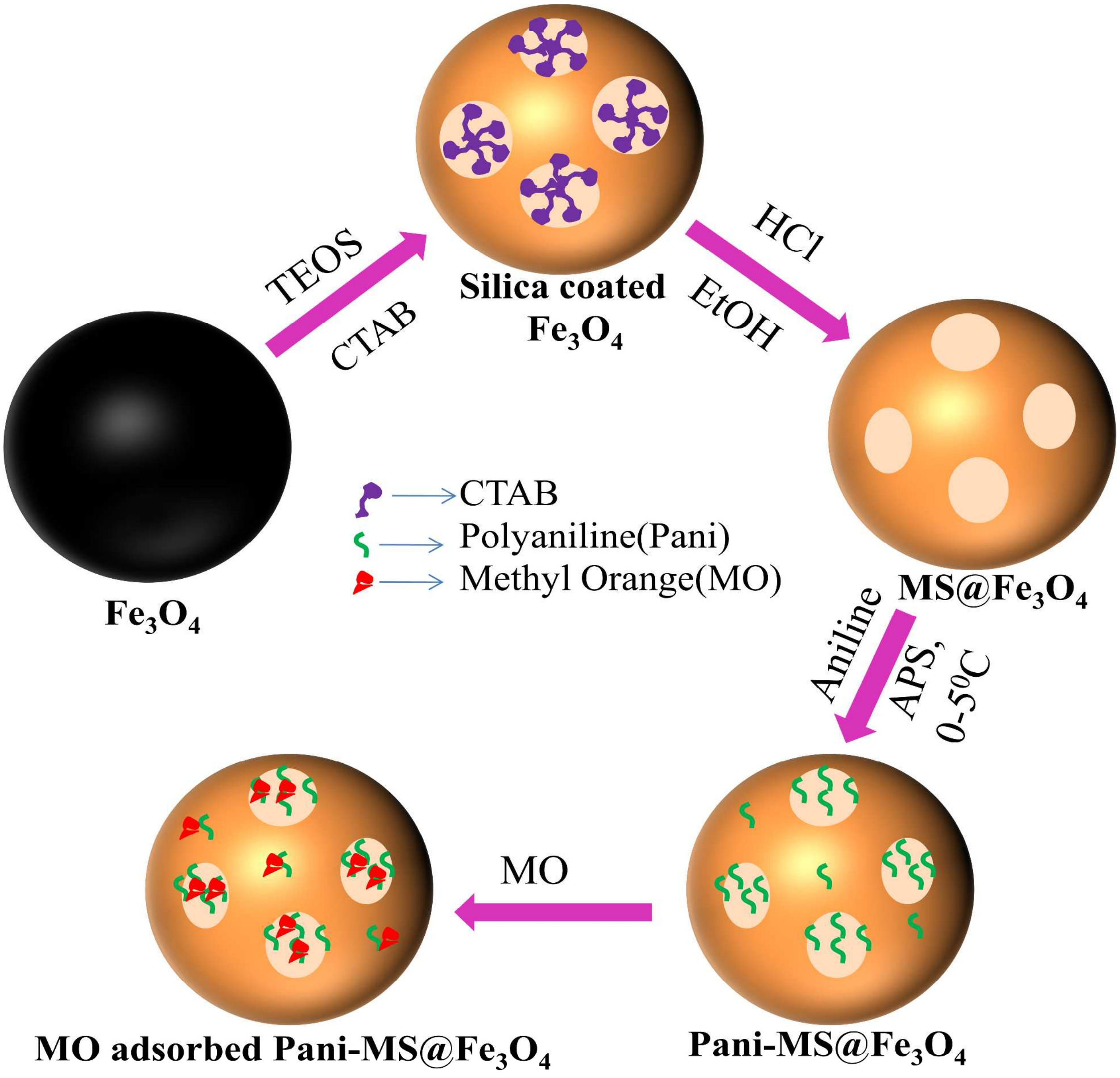

RSC Advances Accepted Manuscript